CHAPTER

Retinal vascular analysis: Segmentation, tracing, and beyond

6

Li Cheng[a,b], Xingzheng Lyu[c], He Zhao[d], Huazhu Fu[e], Huiqi Li[d]

[a]*A*STAR, Bioinformatics Institute, Singapore, Singapore*

[b]*ECE, University of Alberta, Edmonton, AB, Canada*

[c]*Zhejiang University, Hangzhou, China*

[d]*Beijing Institute of Technology, Beijing, China*

[e]*A*STAR, Institute for Infocomm Research, Singapore, Singapore*

1 Introduction

As the proverb goes, the eye is a window to your soul. In fact, the eye is also a window to your health, as many diseases such as eye diseases, diabetes, cardiovascular, and systemic diseases manifest themselves via different structures, especially the blood vessels, in an eye. For example, it is of clinical interest to examine the width of artery or vein vessels, the branching ratio, the vessel length between junction points, etc. As illustrated in, for example, Ref. [1], stemmed from the ophthalmic artery, the arterial inflow to the eye is further branched. In particular, the central retinal artery travels along the optic nerve and spreads out in branches to cover the retina. Being parallel and countercurrent to the central retinal artery, the venous outflow exits the eye through the central retinal vein, again along the optic nerve. Together, the retinal vasculature is responsible for supplying oxygen and nutrients and removing metabolic waste from the retina. Impaired oxygen supply can as well damage the health of the retina.

Readouts from vessel structure or vasculature have been linked to various diseases. Subtle vessel changes may also occur during the early stage of disease cycle. The departure of vasculature geometry from normal state may also underlie the development of other signs such as retinal lesions. For example, it is known that the vasculature geometry including vessel diameter and tortuosity provide predictive information for hypertension, diabetes, Alzheimer disease, and cardiovascular disease [2–8]. It is thus used frequently in reliable and automated procedures in analyzing the vasculature and its associated properties. This chapter will focus on

Computational Retinal Image Analysis. https://doi.org/10.1016/B978-0-08-102816-2.00006-X

analyzing vessel structure in retinal images. Note that there also exist artery and vein branches that serve the rest part of the eye including cornea and iris, which are not the main theme of this chapter.

Retinal imaging has been around for over a hundred years, with the first instrument being invented in 1851 [9] and the first practical fundus camera developed in 1921 by Gullstrand who was later awarded Nobel Prize for this contribution. Recently, color fundus (CF) photography and optical coherence tomography (OCT) are among the noninvasive and popular clinical choices.

Vasculature analysis in retinal images has, therefore, a longstanding history. Arguably the first research effort was by Matsui et al. [10], 45 years ago, where a mathematical morphology approach is construed toward the problem of vessel segmentation. Overall, there has been relatively sporadic research efforts in the 1970s and 1980s. In particular, the work of Akita and Kuga [11] considers building up a holistic approach for understanding retinal fundus images, including segmenting retinal blood vessels and recognizing individual artery and vein trees, and detecting vessel structural changes such as arteriovenous nicking (AVN). Their efforts were ambitious even by current standards, since each of the tasks is typically pursued by a separate research paper today. The review paper by Gilchrist [12] summarizes these early research activities. Since the 1990s, the research activities in retinal vasculature image analysis start to proliferate, mostly owing to the change of clinical practice in wide-spread adoption of digital retinal imaging. Over the years, it has resulted in an enormous amount of literature on wide-spread-related topics. In this chapter, we strive to provide an up-to-date account, focusing more on the recent progresses and challenges in retinal vessel analysis perspective, especially about the problems of vessel segmentation, tracing, and classification, as, for example, shown in Fig. 1 on CF images. Regarding the related topics, such as retinal image quality assessment, registration and stitching of overlapping retinal images, segmentation of fovea/macular and optic disk (OD), lesion detection and segmentation, and OCT-based segmentation and analysis, they are covered by other chapters of this book. There are also review articles: in Ref. [13], Abramoff and coworkers provide an excellent overview of the history up to 2010, current status, and future perspective in both retinal imaging and image analyses. While the survey of Kirbas and Quek [14] is from the general perspective of segmenting and tracing vessels, the review articles of Fraz et al. [15] and Almotiri et al. [16] focus specifically on retinal vessel segmentation. Miri et al. [17] conduct a comprehensive study of retinal vessel classification. Meanwhile, the reviews by Faust et al. [18] and Mookiah et al. [19] are dedicated to image-based detecting and diagnosing of diabetic retinopathy disease, respectively. The knowledge of retinal scans and vasculature analysis could also be helpful in robot-assisted eye surgery [20,21]. In addition to medical applications, retinal vasculature analysis has also been used for biometrics and authentication purposes, see, for example, Refs. [22,23].

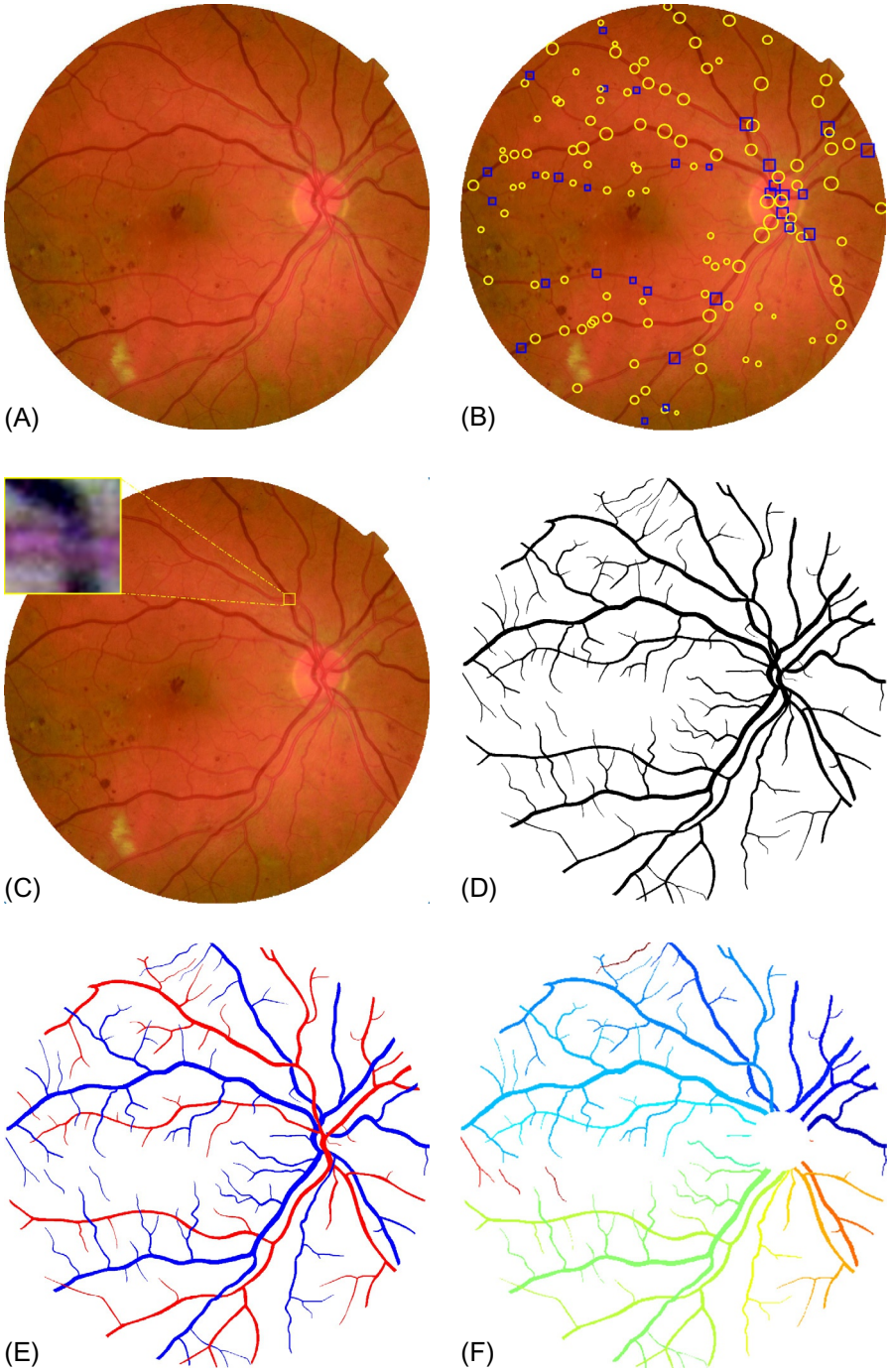

FIG. 1

Typical retinal vascular annotations of a color fundus image. Panel (A) is an original retinal fundus image. Panel (B) marks out the bifurcation and crossing points by *yellow circles* and *blue rectangles*, respectively. Panel (C) highlights the AVN signature in panel (A), with a *zoomed-in inlet* showing an enhanced image patch by subtracting local mean image from the raw image. Panel (D) presents an annotation of blood vessel segmentation, which is classified into artery and vein vessels in panel (E). Panel (F) displays the individual vascular trees, each with a unique color.

2 Benchmark datasets and evaluation metrics

2.1 Datasets

Table 1 provides a summary of 12 representative retinal imaging benchmark datasets. As some URLs of these published datasets are relocated over the years, we strived to identify the current web addresses.

DRIVE[1] [24] and STARE[2] [25] are two popular benchmarks for vessel segmentation. DRIVE contains 40 fundus images of size 768 × 584, obtained using Canon CR5 nonmydriatic 3CCD camera with field of view (FOV) of 45 degrees. STARE involves 20 fundus images of size 605 × 700 taken from a TopCon TRV-50 fundus camera at 35-degree FOV. Apart from segmented vessel masks, the artery/vein vessel annotations are further labeled by RITE[3] [26, 27] for DRIVE dataset. Azzopardi and Petkov [28] provided vessel junction annotations, including vascular bifurcations and crossovers.

HRF[4] [29] consists of 45 images, of which one-third are images from healthy patients, one-third are patients with diabetic retinopathy (DR), and the rest are images of glaucomatous patients. Binary gold standard vessel segmentation images, generated by a group of experts, are available for each image. The size of fundus images is 3504 × 2336.

CHASEDB1[5] [30] includes 28 retinal fundus scans from 14 children. Images were recorded using a Nidek NM-200-D fundus camera with a 30-degree FOV, with a resolution of 999 × 960 pixels. Two experts' segmentations are available for each images as ground truth.

ARIA[6] [31] consists of 143 images taken from either healthy subjects, diabetics, or patients with age-related macular degeneration (AMD). Obtained with a Zeiss FF450+ fundus camera with a 50-degree FOV. In addition to vessel segmentation, annotations of the OD and fovea are also provided.

The DR HAGIS[7] [32] dataset is composed of 40 fundus images, which were acquired in different screening centers in the United Kingdom for DR screening purpose, using a Topcon TRC-NW6s, a Topcon TRC-NW8, or a Canon CR DGi fundus camera with a horizontal 45-degree FOV. The resulting images are of different sizes, being either 4752 × 3168, 3456 × 2304, 3126 × 2136, 2896 × 1944, or 2816 × 1880 pixels. The dataset is divided into four comorbidity subgroups, that is, DR, hypertension, AMD, and glaucoma. Each subgroup comprises 10 images, with the image of only one patient being duplicated into two subgroups. Vessel segmentation annotation is also provided for each image.

[1] See http://www.isi.uu.nl/Research/Databases/DRIVE/.
[2] See http://www.ces.clemson.edu/~ahoover/stare/.
[3] See https://medicine.uiowa.edu/eye/rite-dataset.
[4] See https://www5.cs.fau.de/research/data/fundus-images/.
[5] See https://blogs.kingston.ac.uk/retinal/chasedb1/.
[6] See https://eyecharity.weebly.com/aria_online.html.
[7] See https://personalpages.manchester.ac.uk/staff/niall.p.mcloughlin/.

Table 1 A summary of representative retinal image datasets and benchmarks.

Database	IT	No. of images	Vessel masks	Vessel trees[a]	A/V	Junctions	Tortuosity	AVR
DRIVE [24]	CF	40	✓	✓	✓	✓		
STARE [25]	CF	20	✓					
HRF [29]	CF	45	✓					
CHASEDB1 [30]	CF	28	✓					
ARIA [31]	CF	143	✓					
DR HAGIS [32]	CF	40	✓					
VICAVR	CF	58	✓	✓	✓			
INSPIRE-AVR [33]	CF	40		✓	✓			✓
RVTD [34]	CF	60			✓		✓	
IOSTAR [35]	SLO	24	✓	✓	✓			
AV-WIDE [36]	UWFI	30		✓	✓			
VAMPIRE [37]	FA	8	✓					

Notes: For retinal imaging technique (IT), CF refers to color fundus photography, SLO is for scanning laser ophthalmoscopy, FA is for fluorescein angiogram, and UWFI is for ultra-wide fundus imaging. "Vessel masks" denotes vessel segmentation annotation, while "Vessel trees" is for annotation of individual vessel trees, and "A/V" stands for artery and vein vessel annotations. "Junctions" is bifurcation and crossing labeling. "Tortuosity" and "AVR" are two clinical relevant vessel readouts (see Section 4.4 for details).

[a]For DRIVE, IOSTAR, VICAVR, and INSPIRE-AVR, individual vessel trees out of the OD are manually annotated and make available online (http://imed.nimte.ac.cn/vetovessel-topology-groundtruth.html).

The dataset of VICAVR[8] includes 58 images, acquired by a TopCon NW-100 nonmydriatic camera with a resolution of 768 × 584. Annotated vascular patterns include the caliber of the vessels measured at different radii from the optic disc as well as the vessel type (artery/vein) labeled by three experts.

INSPIRE-AVR[9] [33] has 40 images of 2392 × 2048 pixels and corresponding arteriolar-to-venular diameter ratio (AVR) values observed by two ophthalmologists. The artery/vein vessel centerlines and the vessel types are further labeled by Dashtbozorg et al. [27].

RVTD[10] [34] is for vascular tortuosity evaluation. It contains 60 zoomed images with 30 arteries and 30 veins that are ranked by vessel tortuosity. These image patches are extracted from 60 retinal images with 50-degree FOV and 1300 × 1100 pixels.

In addition to the typical CF photography, there are also benchmarks on different retinal imaging devices, including scanning laser ophthalmoscopy (SLO), ultra-wide fundus imaging (UWFI), and fluorescein angiogram (FA).

- IOSTAR[11] [35] includes 24 images, vessel segmentation, artery/vein, and OD annotations. Images are acquired with an EasyScan SLO camera with a 45-degree FOV.
- AV-WIDE[12] [36] has 30 ultra-wide FOV images, includes both healthy eyes as well as eyes with AMD. Each image is from a different individual, was obtained using obtained using an Optos 200Tx UWFI camera, and is of around 900 × 1400 in size. Annotations of the vessel segmentation and the artery-vein labels are provided.
- VAMPIRE[13] [37] contains eight ultra-wide FOV FA images, obtained from OPTOS SLO ultra-wide FOV device which may achieve up to 200-degree FOV with scanning SLO technique. These images were taken from two different FA image sequences, with vessel segmentation annotation being provided.

Fig. 1 shows a CF image and various vessel annotations, including vascular junctions, vessel segmented, artery/vein, and tree masks. Meanwhile, there are also efforts in applying multispectral imaging to retinal studies. For example, CMIF[14] [38] is a dedicated multispectral fundus image dataset of 35 sets of images from 35 healthy young individuals of diverse ethnicities. The multispectral images are acquired by implementing a filter wheel into fundus camera, which gives rise to a set of 17 narrow band-pass filters for designated wavelengths in the range of 480–705 nm. This development is yet to be ready for clinical translation, nevertheless it offers novel insights into retinopathy.

[8] See http://www.varpa.es/research/ophtalmology.html.
[9] See https://medicine.uiowa.edu/eye/inspire-datasets.
[10] See http://bioimlab.dei.unipd.it/RetinalVesselTortuosity.htm.
[11] See http://www.retinacheck.org/datasets.
[12] See http://people.duke.edu/~sf59/Estrada_TMI_2015_dataset.htm.
[13] See https://vampire.computing.dundee.ac.uk/vesselseg.html.
[14] See http://www.cs.bham.ac.uk/research/projects/fundus-multispectral/.

As shown in Table 1, the number of images in each dataset ranges from 8 to 143. The typical dataset size is often several order-of-magnitude smaller when comparing to the popular image detection/segmentation benchmarks used in the broader computer vision community, such as ImageNet [39] and COCO [40] that typical have 20–200 K images or more in the training and validation sets. In a sense, this dataset characteristic makes the practical situation less appealing. The situation is especially pronounced when deep learning methods such as convolutional neural networks (CNN) are engaged, as CNN models often require access to large and well-annotated training set. The CNN models trained in the retinal datasets thus tend to be less robust, and tend to be more vulnerable to small perturbation of input images or adversarial attacks at test run.

2.2 Evaluation metrics

With the increasing amount of activities toward vessel segmentation and tracing, there is naturally a demand for proper evaluation metrics, where different methods can be compared quantitatively and objectively on the same ground. The typical metrics are usually individual pixel-based, which including, for example, the precision-recall curve, and the F1 score as a single-value performance indicator. The sensitivity and specificity pair could be another popular choice. It is worth noting that the commonly used metric of receiver operating characteristic curve or ROC curve may not be suitable in our situation here, since the positive vessel and negative background pixels or examples are severely imbalanced. As a well-established mean to globally quantify pixel-based deviations, a major drawback of this type of metrics is that the vasculature geometric information is not well preserved in evaluation. This motives the construction of structural type of metrics [41–43] to best account for the differences from vasculature geometry perspective. The metric considered in Ref. [41] places more emphasis toward the aspects of both detection rate and detection accuracy, where the vascular structures between the predicted and the reference are optimally matched as a solution to the induced maximum-cardinality minimum-cost graph matching problem. Meanwhile, the structural metric proposed by Gegundez-Arias et al. [42] involves the comparison of three aspects between the predicted vessel segmentation and the corresponding reference annotation, namely number, overlap, and length. Number refers to comparing the number of connected segments presented in prediction as well as in the annotation images. Overlap is to assess the amount of overlaps between the predicted segmentation and the reference annotation. Length is to examine the length similarity between the predicted and the annotated vessel skeletons. In a more recent attempt [43], a structural similarity score is designed to incorporate both location and thickness differences that the segmentation is departed from the reference vessel trees. A very detailed discussion on validation of retinal image analysis can be found in Ref. [44]. See also Chapter 9 in this book for a discussion on validation techniques.

In addition to the aforementioned situation where there exists full annotations in the dataset for performance evaluation, there are often practical vessel segmentation

scenarios when no reference is available. This is tackled by, for example, the paper of Galdran et al. [45], where a similarity metric is presented to quantify the segmentation performance in the absence of reference annotation. A web-based client-server system is described in Ref. [46], which consists of a component for vessel tracing, an interactive editing interface for refining parameters and fixing prediction errors, and a component responsible for outputting the clinical indexes.

3 Vessel segmentation

It is often of foremost interest to segment the retinal blood vessels pixel by pixel in a retinal image, corresponding to the blood column within the vessels. An example of vessel segmentation on CF images is shown in Fig. 1D.

Existing methods can be roughly divided into two categories based on whether an annotated training set is required: unsupervised and supervised methods. While supervised methods learn their models based on a set of training examples, unsupervised methods do not require a training set.

3.1 Unsupervised segmentation

As mentioned, arguably the first research effort of retinal segmentation is by Matsui et al. [10], 45 years ago, where a mathematical morphology approach is taken toward the problem of vessel segmentation.

Matched filtering and mathematical morphology-based techniques were popular choices in the early days. In Ref. [47], Chaudhuri et al. approximate the vessel segment profiles by a set of 1D Gaussian shaped filters over various spatial directions. As part of an initiative at the Vienna Eye Clinic for diagnosis and treatment of AMD, a dedicated pipeline is presented [48] to analyze retinal images based on SLO. In addition to separate modules for detecting the optic disk, fovea, and scotoma locations, its vessel segmentation module operates by matching the prototype zero-crossing of the gradient profiles and applying grouping. Hoover et al. [25] discuss the application of 12 Gaussian shape-matched filters in 2D, which produces a response image recording the highest response at each pixel. This is followed by a sequence of carefully designed threshold probing steps to produce the predicted segmentation. The STARE dataset is introduced in this paper. A second-order Gaussian matched filtering approach is considered by Gang et al. [49] to detect vessels. The work of Staal et al. [24] focuses on extracting the centerlines or ridges of the 2D vessels, which is achieved by means of a *k*-nearest neighbor classifier and sequential forward feature selection-based method. Importantly, it contributes the widely used DRIVE dataset. A set of three vessel detection variants are studied in Ref. [50] to account for noisy input images. The methods are derived from the likelihood ratio test in making local decisions, and model selection for choosing the optimal intrinsic parameters. A supervised likelihood ratio test is developed in Ref. [51] that combines matched-filter responses, and customized measures of confidence and vessel boundary-ness.

A systematic approach is conducted in Ref. [52], where vessel structure is segmented using morphological operators, based on which the OD and macular are then localized by likelihood ratio tests. Mendonca et al. [53] use four directional differential operators to detect the vessel centerlines, which then facilitate the morphological reconstruction of vessels. The work of Miri and Mahloojifar [54] proposes to use curvelet transform and morphology operators for edge enhancement, then apply a simple threshold along with connected components analysis for delivering the final segmentation. Martinez-Perez et al. [55] conduct segmentation by a combination of multiscale analysis of gradient and Hessian information and region-growing approach. A multiresolution 2D Hermite model is investigated in Ref. [56], where a quad-tree is used to organize the spatial configuration, an expectation-maximization type optimization procedure is developed to estimate the model parameters. Moreover, Bankhead et al. [57] utilize isotropic undecimated wavelet transform for unsupervised segmentation. In segmenting UWFI Fundus FA images, Perez-Rovira et al. [37] employ steerable filters and adaptive thresholding. An iterative approach is devised in Ref. [58] to include new vessel structures by local adaptive thresholds. A similar strategy is also considered by Xu et al. [59], where a tree-structured shape space is considered and for retinal vessel segmentation, local threshold is applied recursively. The work of Kovacs and Hajdu [60] advocates a two-step process. First, generalized Garbor filter-based template matching is used to extract the centerlines. Second, iterative contour reconstruction is carried out based on the intensity characteristics of the vessel contours.

Variational methods have been another popular line of techniques in retinal vascular segmentation. A deformable contour model is adopted by Espona et al. [61], by incorporating the snake method with domain-specific knowledge such as the topological properties of blood vessels. In Ref. [62], a dedicated active contour model is developed that uses two pairs of contours to capture each side of the vessel edges. To address the challenging pathological images, Lam and Yan [63] investigate the application of divergence operator in the gradient vector field. Moreover, to deal with the issue of multiconcavity in the intensity profile of especially pathological fundus images, a variational approach is taken in Ref. [64] based on perceptual transform and regularization-based techniques. An active contour model with local morphology fitting is discussed in Ref. [65] to segment vessels in 2D angiogram. The combined use of regional information and active contour techniques is further considered in Refs. [66, 67]. In Ref. [35], new filters are proposed based on lifting a 2D image is lifted by Lie-group into a 3D orientation score, and by applying multiscale second-order Gaussian derivatives, and follow-up eigensystem analysis of the left-invariant Hessian matrix. After projecting back from 3D space to 2D image plane, the segmentation result is obtained by applying a global threshold. Recently, a minimal path approach is reported in Ref. [68], where a dynamic Riemannian metric is updated during the course of a single-pass fast marching method. It is sometimes advantageous to perform interactive image analysis. This is addressed by Poon et al. [69], where a multiscale filtering approach is designed to simultaneously compute centerlines and boundaries of the retinal vessels.

Other techniques also exist. For example, by establishing an analogy between quantum mechanics and image processing, it is proposed in Ref. [70] to transform image pixels to quantum systems such that they can be evolved from an initial state to a final state governed by the Schrodinger equation.

3.2 Supervised segmentation

The alternative to the unsupervised paradigms are learning-based methods, in which a set of training examples is provided to learn a model that is expected to segment input retinal images at test time as well as the performance it has gained during training. One early work is that of Akita and Kuga [11], where neural networks are used in segmenting retinal vasculature. A system is developed in Ref. [71], where a patch-based neural network model is learned by backpropagation to classify each pixel as being vessel or not, then OD and fovea regions are obtained via template matching.

A typical supervised approach is to first construct or develop a set of dedicated features or filters, then to build a statistical model based on the features as sufficient statistics, with model parameters being estimated (i.e., learned) from a set of training examples. For example, a local patch-based approach is considered in Ref. [72], where an AdaBoost classifier is in place to work with 41 features extracted from the local image patch of the current pixel, where the pixel is to be predicted as being either vessel or not. Martin et al. [73] devise gray-level and moment invariants-based features for segmenting the retinal vessels using neural networks. Ricci et al. [74] work with orthogonal line operators and support vector machine to perform pixel-wise segmentation. Becker et al. [75] present a discriminative method to learn convolutional features using gradient boosting regression technology. In Ref. [76], a pool of difference-of-Gaussian (DoG) filters is used that after training, filters are adaptively selected to best fit the current vessel of interest. A learning-based DoGs filtering approach is proposed in Ref. [77], with one application focus being about the detection of vascular junction points, where orientation is achieved via shifting operations. Empirically it is shown robust to contrast variations and the presence of noises. Furthermore, many learning-based methods [78–81] also advocate the automation of the feature learning process. For example, Soares et al. [78] elaborate upon 18-dimensional Gabor response features to train two Gaussian mixture models (GMMs), which are further employed to produce a binary probability map for a test image. The method of Becker et al. [81] employs a gradient boosting framework to optimize filters and often produces impressive performance.

Several learning paradigms, including graphical models and ensemble learning, are presented with very promising results. A discriminatively trained, fully connected CRF approach is developed by Orlando and Blaschko [82]. This is followed by Orlando [83] with more expressive features in their fully connected CRF model. Besides, the work of Fraz et al. [30] showcases an ensemble classification approach consisting of bagged and boosted decision trees, with features from a variety of aspects including orientations of local gradients, morphological transformations, and Gabor filter responses.

Instead of segmenting vessel pixels directly, a radial projection method is utilized in Ref. [84] to locate centerlines, based on steerable wavelet filtered output of a fundus image. Meanwhile, a semisupervised learning step extracts the remaining vessel structures. Similarly, an iterative algorithm is introduced by Gu and Cheng [85], where starting from the main vessel trunk, small and thin vessel branches and difficult regions around the boundaries are iteratively refined by retrieving and executing a proper local gradient Boosting classifiers, which is stored in a latent classification tree model constructed by Chow-Liu method.

3.3 Deep learning

As a particular supervised segmentation paradigm, a number of end-to-end deep learning approaches have been developed in our problem scenario with notable performance improvements. The N4-field [86], as an example, combines the CNN with nearest neighbor search to detect local patches of natural edges as well as thin and long objects. A CNN model is also trained in Ref. [87] based on 400,000 preprocessed image patches obtained from the training sets of DRIVE, STARE, or CHASEDB1 datasets, which are essential for ensuring reliable test performance. Similarly, a deep neural network is used by Li et al. [88] to model the cross-modality data transform for vessel segmentation in retinal images. Fu et al. [89] propose to incorporate both CNN and CRF models for segmenting the full input fundus image. The deep learning approach of Yan et al. [90] incorporates both conventional pixel-wise loss and segment-level loss terms to achieve a globally plausible solution. In addition, as demonstrated with the impressive performance in Ref. [91], it is possible to address multiple tasks jointly, including vessel segmentation and, for example, optic disk detection.

There exists, however, one major issue with the current segmentation task. DRIVE (40 annotated images) and STARE (20 annotated images) datasets have been the de facto benchmark in empirical examination of retinal image segmentation techniques. Meanwhile, annotations from, DRIVE and STARE are from multiple medical experts, which result in different reference (“gold”) standards. The disagreement from multiple experts may be attributed to the inevitable subjectiveness and variability of expert judgment. It also reflects the difficulty level of the task and the reliability of the gold standard in the context. As our algorithms are approaching human-level performance, it becomes increasingly difficult to quantitatively validate new algorithms, as the vessels produced by these methods on test images are more agreeable to the particular reference standard they are trained with, when comparing with the other reference standards. This suggests an overall performance saturation of the current benchmark, most possibly due to the small dataset size, and stresses the need for larger benchmark datasets. Some steps have been taken toward addressing this concern. Among them, it is shown in Ref. [92] that the retinal segmentation performance can be improved by incorporated (potentially infinitely many) synthesized images into the typically small training set. An even more challenging problem is performing fundus image segmentation on a new and distinct fundus image dataset in the absence of manual

annotations. To address this problem, Zhao et al. [93] present a supervised learning pipeline. The key is the construction of a synthetic retinal image dataset capable of bridging the gap between an existing reference dataset (where annotated vessel structures are available) and the new query dataset (where no annotation is available). Then existing supervised learning segmentation methods are to be engaged to learn a model dedicated to the set of query images.

Due to the visual similarity between retinal vessels from, for example, fundus imaging and neurons from, for example, confocal microscope, there are also many efforts in devising algorithms to address the more general problem of segmenting such tubular structured objects [85, 94–100], with retinal blood vessel being a special case. For example, the well-known local Hessian-based vessel enhancement method developed by Frangi et al. [94] has been widely used for segmenting both 2D and 3D vessels. A mathematical morphology and curvature evaluation-based method was developed by Zana and Klein [95] to segment the vessel-like structures from background. Minimal path techniques are considered in a series of closely related efforts [101–103] to connect vessel segments in 2D or 3D. The work of Benmansour and Cohen [96] also addresses generic 2D and 3D segmentation of tubular structured objects in images, with an interactive method using minimal path and anisotropic enhancement. A multiscale centerline detection method is presented in Ref. [98] based on learned filters and GradientBoost regression technique. The method of Gu et al. [100] attempts to capture structural and contextual features from fundus images through their proposed data-driven feature learning procedure.

4 Vessel tracing

The topological and geometrical properties of retinal vessel trees are vital in screening for and diagnosing diseases, which call for proper tracing of the individual vessel trees from fundus images. The problem of vessel tracing is more than segmentation where vessel pixels are separated from the backgrounds, in that we would like to first separate artery and vein vessels, as shown in Fig. 1E. An equivalent problem is to detect junctions and decide as being either branching or crossing. Individual vessel trees usually could be distinguished from the rim of the optic disk, as shown in Fig. 1F, thus we answer the question of which pixel belongs to which of the vessel trees.

4.1 Vascular junction identification

Detecting and categorizing the junction points into either bifurcation or crossing is useful in vessel tree extraction and classification. Fig. 1B illustrates an exemplar annotation of such bifurcation and crossing points. In one of the early efforts, a morphological-type edge detection algorithm is used in Ref. [104] to automate the recognition of arteriovenous intersections. An image processing-based approach is considered in Ref. [105] that first extracts the vessels by preprocessing filtering

and *k*-means, then utilizes a combined cross-point number method for thinning, and pattern-matching classification of the junction points as either branching or crossover. Calvo et al. [106] consider the detection and classification of key points pertaining to bifurcations and crossovers in the retinal vessel trees. A two-step method is proposed, which uses filters and morphologic operations for detection, and the extracted key point-based features for classification into either bifurcations or crossovers. Started with a segmented retinal image, Azzopardi and Petkov [28] deploy a set of blurred and shifted Gabor filters that are trained from a set of predefined bifurcation prototypes, and demonstrate satisfactory detection performance on DRIVE and STARE datasets. In addition to their initial work [107] where self-organizing feature maps are used to perceptually group the retinal segments around the junction points, Qureshi et al. [108] develop a probabilistic model of various junction points such as terminals, bridges, and bifurcations, and their configurations.

4.2 Vascular tree separation

The work of Tamura et al. [109] is among the early efforts, where the blood vessels are traced by a second-order derivative Gaussian filter from an initial point, while the width of the blood vessel is obtained as the zero-crossing interval of the filter output. Similarly, starting from a set of initial points, the work of Can et al. [110] tracks vessels by recursively applying a set of directional low-pass filters to the proper directions along the vessel centerlines detected so far from the input retinal angiogram images. It also extracts the branching and crossover points as a by-product. A three-step approach is proposed in Ref. [111] to reliably detect vascular bifurcations and crossovers, which involves initialization of junction locations, iterative estimation, and backtrace-based refinement.

Kalman filter-based tracking method could be a natural choice, which has been considered by, for example, Yedidya and Hartley [112]. To reconstruct individual retinal vascular trees, Lin et al. [113] start by spreading initial seeds along the vessels. The vessel segments are then extracted via a likelihood ratio test. At a junction point, the vessel tree assignment is then resolved by applying a locally minimum-cost matching as well as extended Kalman filtering.

One important observation is that both local and global contexts are helpful in resolving the bifurcation and crossover issue. For example, at a junction, it is valuable to examine the angular, morphological, and textural properties of all segments at the junction. In fact, the inclusion of information from nearby junctions could also facilitate a better local decision at current junction. This line of thoughts inspires the graph-based formulation where each vessel segment becomes a node, and a contact between two adjacent segments is represented by an edge between the two nodes. This naturally leads to an undirected graph representation. The tracing problem has been thus formulated as an inference problem in a Markov random field [114], a label propagation problem on undirected graphs [115], or directed graphs [116–118]. Similar graph-based methods are also adopted in Refs. [119, 120].

Variational approaches have also been considered in this context. Inspired biologically by the cortical orientation columns in primary visual cortex, Bekkers et al. [121] advocate a special Euclidean group, SE(2), on which to base their retinal vessel tracking system. Bekkers and co-workers subsequently introduce an interesting differential geometry approach [122], where vessel tracing is formulated as sub-Riemannian geodesics on a projective line bundle. This is further investigated in Ref. [123] as a nilpotent approximations of sub-Riemannian distances for fast perceptual grouping of blood vessels in 2D and 3D. Abbasi-Sureshjani et al. [124] consider a 5D kernel approach obtained as the fundamental solution of the Fokker-Planck equation to deal with the presence of interrupted lines or highly curved blood vessels in retinal images. A mathematical contour completion scheme is proposed by Zhang et al. [125] based on the rotational-translational group SE(2). The original 2D disconnected vessel segments are lifted to a 3D space of 2D location and an orientation, where crossing and bifurcations can be separated by their distinct orientations. The contour completion problem can then be characterized by left-invariant PDE solutions of the convection-diffusion process on SE(2).

The tracing problem has indeed attracted research attentions from diverse perspectives that go beyond the paradigms mentioned so far. In terms of deep learning, the work of Ventura et al. [126] extracts the retinal artery and vein vessel networks by iteratively predicting the local connectivity from image patches using deep CNN. Uslu and Bharath [127] consider a multitask neural network approach to detect junctions in retinal vasculature, which is empirically examined in DRIVE and IOSTAR benchmarks with satisfactory results. A fluid dynamic approach is introduced in Ref. [128] to determine the connectivity of overlapping venous and arterial vessels in fundus images. Moreover, aiming to balance the trade-off between performance and real-time computation budget, Shen et al. design and analyze in Ref. [129] the optimal scheduling principle in achieving early yield of tracing the vasculature and extracting crossing and branching junctions. It is also worth mentioning that similar problem has also been encountered by the neuronal image analysis community with numerous studies of datasets and methods [130–132]. There are also efforts in addressing the more general problem of tracing tubular structured objects that include retinal vessel tracing as a special case [117,118,126].

4.3 Arterial/venous vessel classification

The classification of blood vessels into arterioles and venules is a fundamental step in retinal vasculature analysis, and is a basis of clinical measurement calculation, such as AVR. This requires not only identifying individual vessel trees, but also assigning each vessel tree as being formed by either arteries or veins. Interested readers may consult Miri et al. [17] for a detailed review of this subject.

As an early research effort, Akita and Kuga [11] consider the propagation of artery/vein labeling by a structure-based relaxation scheme on the underlying vascular graph. A vessel tracking method is presented in Ref. [111] to resolve the connectivity issues of bifurcations and crossings. A semiautomatic system

is described in Ref. [133], consisting of segmenting the vessel pixels, thinning to obtain vessel skeletons, and tracking individual vessel trees. As a result, a number of geometric and topological properties are subsequently quantified, which include vessel segment lengths, diameters, branching ratios, and angles. In Ref. [134], the problem of artery versus vein separation from a vascular graph is cast as a SAT-problem, where a heuristic AC-3 algorithm is utilized to address a double-layered constrained search problem. Instead of working with fundus image of a single wavelength, it is considered in Ref. [135] to work with a specific fundus imaging set-up that acquires two images simultaneously, at different wavelengths of 570 and 600 nm, respectively. By exploiting the difference between artery and vein vessels that have distinct central reflex patterns, an SVM classification-based method is proposed to identify the vessel types. A multistep pipeline is considered in Ref. [136]. First, a vesselness value is computed for each pixel, which forms a vessel score image. Then points are sampled from local maxima points of the score image, and these points are linked into spanning trees by solving the induced k-cardinality arborescence problem with ant colony optimization-based algorithm. Based on 27 hand-crafted features, a linear discriminant classifier is used in the work of Niemeijer et al. [33] to classify vessel segments into arteries and veins. In Ref. [26], Hu et al. use a graph-based metaheuristic algorithm to segment and separate a fundus image into multiple anatomical trees, while the RITE dataset is also constructed. In Ref. [27], the classification of artery versus vein vessel segments is carried out based on the analysis of a graph extracted from the retinal vasculature, where the annotation of annotate artery and vein vessels is also provided for both DRIVE and INSPIRE-AVR datasets. For ultra-wide field SLO, Pellegrini et al. [137] also consider a graph-cut-based approach, where the node and edge-related features are manually designed features based on local vessel intensity and vascular morphology. A system is developed in Ref. [138] to segment vessels by Otsu binary thresholding, and obtain skeleton by applying mathematical morphology. This is followed by localization of branch points, crossing points, and end points. As a result, a graph structure is formed, and the Dijkstra algorithm is used to search vessel subtrees by minimizing the accumulative edge costs. Finally, a k-means clustering algorithm is executed to separate artery and vein subtrees.

Targeting at wide-FOV images, a planar graph-based method is considered by Estrada et al. [36] in constructing a likelihood model to take into account the prior knowledge regarding color, overlap, and local growth aspects of vessel segments at junctions. A heuristic search is thus carried out for optimal separation of the artery and vein vessel trees.

4.4 Clinical relevant vessel readouts

Retinal vascular abnormalities, for example widening or narrowing of retina blood vessels and increased vascular tortuosity, provide significant hints on various diseases, such as diabetes, hypertension, and coronary heart disease. Measurements to quantify retinal vascular changes are as follow:

Diameter changes. AVR, AVN, and FAN are three quantification measurements of diameter changes. AVR calculation is restricted to an area of 0.5–1.0 disc diameters from the OD. An automated pipeline is presented in Ref. [139], which segments and skeletonizes the vessels, and classifies arterial/venous vessel segments that are separated at the junction points. The six widest artery and vein segments are selected for AVR calculation, which is measured by an iterative algorithm. AVN is a phenomenon where venular caliber decreases as an arteriole crosses over a venule. A four-level grading approach of AVN is proposed in Ref. [140]. FAN refers to arterial vascular segment whose diameter $\geq$50 μm narrows. Severity degree of FAN is evaluated by the length of narrowing vessels compared with the diameter of OD.
Tortuosity alteration. This is an early indicator of a number of vascular diseases. Some of tortuosity quantification of arteries and veins approaches are (1) tortuous or nontortuous classification; (2) tortuosity ranking of vessel segments [34]; and (3) tortuosity grading of individual vascular trees [141].

5 Summary and outlook

A significant amount of effor has been devoted to vasculature analysis from retinal images, which have led to noticeable progress in clinical quantifications to improve diagnosis and prognosis of related diseases. There are also a number of promising research directions, some of them discussed in the following sections.

5.1 Vasculature analysis in emerging imaging techniques

We highlight here the emerging retinal imaging techniques referred to as 3D, multimodal, and mobile imaging.

3D vessel analysis. To date, the majority of existing benchmark datasets and research efforts are devoted to segmentation in 2D retinal fundus images. Being a 2D projection of the 3D retinal vasculature, the retinal fundus images contains necessarily only a partial observation of the underlying 3D vessels. Meanwhile, with emerging 3D imaging techniques such as spectral-domain OCT (SD OCT or 3D OCT) and plenoptic ophthalmoscopy [142], we are now capable of imaging the 3D vasculature volume of the retina. It is thus possible to directly extract the 3D retinal vasculature volumes.
The endeavors of Haeker et al. [143] and Garvin et al. [144] are among the first in devising dedicated 3D segmentation techniques for time-domain macular scans. In terms of spectral-domain OCT volumes, the work of Niemeijer et al. [145] considers a *k*-NN pixel classification approach where Gaussian filter banks are used to produce good features. The results are evaluated on the macular centered scans as well as the optical nerve head centered scans. An interactive 3D segmentation approach is developed by Fuller et al. [146].

Moreover, Guimaraes et al. [147] report segmentation and reconstruction of 3D retinal vasculature. With the further advancement of 3D imaging techniques, this exciting direction of 3D vessel analysis possesses excellent research potential. It is also well connected to existing 3D blood vessel analysis efforts of other organs and via different instruments such as magnetic resonance imaging.

Multimodal vessel analysis. One prominent example of multimodal retinal image analysis could be the combined usage of 2D fundus and 3D OCT images in vessel segmentation and tracing. Here, Hu et al. [148] investigate the integration of 2D fundus image and corresponding 3D OCT images in retinal vessel segmentation. SLO fundus image and corresponding macular OCT slices are jointly considered in Ref. [149] in two steps. The first step involves 2D vessel segmentation of fundus images in curvelet domain, with the side information from multiple OCT slices. The second step focuses on 3D reconstruction of the blood vessels from the OCT data. In addition to images, patient-related information such as electronic medical records and genetic data could also be taken into account for better disease diagnosis, and patient prognosis and treatment.

Analyzing mobile retinal images. As stated in Ref. [150], the recent development of portable fundus cameras [151] and smartphone-based fundus imaging systems have led to considerable opportunities as well as new challenges to retinal image analysis, such as the demand for more affordable imaging devices with perhaps lower computation cost [152]. To address the need of the emerging mobile retinal diagnostic devices that calls for segmentation techniques with low memory and computation cost, Hajabdollahi et al. [152] propose to train a simple CNN model-based pruning and quantization of the original full-sized model, that is capable of retaining the performance with much reduced computation and size. Looking forward, we expect further and considerable progresses along this direction.

5.2 Benchmarks and metrics

Benchmark datasets, such as ImageNet [39] and COCO [40], have played a vital role in fueling the recent computer vision breakthroughs. It has been observed that these successful datasets are both of large scale, and richly annotated. For example, over the years, COCO has introduced and aggregated various annotations on categories and shapes of individual objects and stuffs (backgrounds). Currently, it is capable of hosting a broad variety of closely related tasks including instance segmentation, stuff segmentation, object detection, person keypoint localization, as well as image captioning, visual dialog, image attributes, text detection and recognition, among others. By contrast, existing retinal vasculature image datasets, as shown in Table 1, are of small size, and often not richly annotated. While most state-of-the-art results are still reported based on the well-known benchmarks of DRIVE and STARE, the low-resolution images considered in these datasets are considerably lagging behind

nowadays widely available high-resolution retinal imaging in eye clinics. These practical limitation and discrepancy indeed call for the curation of better benchmark sets of large scale, richly annotated, and aligned well with the current retinal imaging practice. One major issue with empirical evaluation lies in the quantification of how much the predicted vessel trees deviate from the reference annotation. A number of structural metrics [41–43] are suggested, yet a consensus from the community is still to be reached.

References

[1] J.W. Kiel, The Ocular Circulation, Morgan & Claypool Life Sciences, San Rafael, CA, 2010.
[2] T. Wong, R. Klein, D. Couper, L. Cooper, E. Shahar, L. Hubbard, M. Wofford, A. Sharrett, Retinal microvascular abnormalities and incident stroke: the atherosclerosis risk in communities study, Lancet 358 (9288) (2001) 1134–1140.
[3] M. Sasongko, T. Wong, T. Nguyen, C. Cheung, J. Shaw, J. Wang, Retinal vascular tortuosity in persons with diabetes and diabetic retinopathy, Diabetologia 54 (9) (2011) 2409–2416.
[4] C. Cheung, E. Lamoureux, M. Ikram, M. Sasongko, J. Ding, Y. Zheng, P. Mitchell, J. Wang, T. Wong, Retinal vascular geometry in Asian persons with diabetes and retinopathy, J. Diabetes Sci. Technol. 6 (3) (2012) 595–605.
[5] N. Witt, T. Wong, A. Hughes, N. Chaturvedi, B. Klein, R. Evans, M. McNamara, S. Thom, R. Klein, Abnormalities of retinal microvascular structure and risk of mortality from ischemic heart disease and stroke, Hypertension 47 (5) (2006) 975–982.
[6] R. Wu, C. Cheung, S. Saw, P. Mitchell, T. Aung, T. Wong, Retinal vascular geometry and glaucoma: the Singapore Malay eye study, Ophthalmology 120 (1) (2013) 77–83.
[7] P. Zhu, F. Huang, F. Lin, Q. Li, Y. Yuan, Z. Gao, F. Chen, The relationship of retinal vessel diameters and fractal dimensions with blood pressure and cardiovascular risk factors, PLoS ONE 9 (9) (2014) 1–10.
[8] C. Cheung, Y. Ong, M. Ikram, S. Ong, X. Li, S. Hilal, J. Catindig, N. Venketasubramanian, P. Yap, D. Seow, C. Chen, T. Wong, Microvascular network alterations in the retina of patients with Alzheimer's disease, Alzheimers Dement 10 (2) (2014) 135–142.
[9] C. Keeler, 150 Years since Babbage's ophthalmoscope, Arch. Ophthalmol. 115 (11) (1997) 1456–1457.
[10] M. Matsui, T. Tashiro, K. Matsumoto, S. Yamamoto, A study on automatic and quantitative diagnosis of fundus photographs. I. Detection of contour line of retinal blood vessel images on color fundus photographs, Nippon Ganka Gakkai Zasshi 77 (8) (1973) 907–918.
[11] K. Akita, H. Kuga, A computer method of understanding ocular fundus images, Pattern Recogn. 15 (6) (1982) 431–443.
[12] J. Gilchrist, Computer processing of ocular photographs—a review, Ophthalmic Physiol. Opt. 7 (4) (1987) 379–386.
[13] M. Abramoff, M. Garvin, M. Sonka, Retinal imaging and image analysis, IEEE Rev. Biomed. Eng. 1 (3) (2010) 169–208.
[14] C. Kirbas, F. Quek, A review of vessel extraction techniques and algorithms, ACM Comput. Surv. 36 (2000) 81–121.

[15] M. Fraz, P. Remagnino, A. Hoppe, B. Uyyanonvara, A. Rudnicka, C. Owen, S. Barman, Blood vessel segmentation methodologies in retinal images—a survey, Comput. Methods Programs Biomed. 108 (1) (2012) 407–433.
[16] J. Almotiri, K. Elleithy, A. Elleithy, Retinal vessels segmentation techniques and algorithms: a survey, Appl. Sci. 8 (2) (2018) 1–31.
[17] M. Miri, Z. Amini, H. Rabbani, R. Kafieh, A comprehensive study of retinal vessel classification methods in fundus images, J. Med. Signals Sens. 7 (2) (2017) 59–70.
[18] O. Faust, U. Acharya, E. Ng, K. Ng, J. Suri, Algorithms for the automated detection of diabetic retinopathy using digital fundus images: a review, J. Med. Syst. 36 (1) (2012) 145–157.
[19] M. Mookiah, U. Acharya, C. Chua, C. Lim, E. Ng, A. Laude, Computer-aided diagnosis of diabetic retinopathy: a review, Comput. Biol. Med. 43 (12) (2013) 2136–2155.
[20] Y. Douven, Retina Tracking for Robot-Assisted Vitreoretinal Surgery (Master's thesis), Eindhoven University of Technology, 2015.
[21] D. Braun, S. Yang, J. Martel, C. Riviere, B. Becker, EyeSLAM: real-time simultaneous localization and mapping of retinal vessels during intraocular microsurgery, Int. J. Med. Robot. 14 (1) (2018) 1–10.
[22] S. Lajevardi, A. Arakala, S. Davis, K. Horadam, Retina verification system based on biometric graph matching, IEEE Trans. Image Process. 22 (9) (2013) 3625–3635.
[23] Z. Waheed, U. Akram, A. Waheed, M. Khan, A. Shaukat, Person identification using vascular and non-vascular retinal features, Comput. Electr. Eng. 53 (2016) 359–371.
[24] J. Staal, M. Abramoff, M. Niemeijer, M. Viergever, B. van Ginneken, Ridge-based vessel segmentation in color images of the retina, IEEE Trans. Med. Imaging 23 (4) (2004) 501–509.
[25] A. Hoover, V. Kouznetsova, M. Goldbaum, Locating blood vessels in retinal images by piecewise threshold probing of a matched filter response, IEEE Trans. Med. Imaging 19 (3) (2000) 203–210.
[26] Q. Hu, M. Abramoff, M. Garvin, Automated separation of binary overlapping trees in low-contrast color retinal images, in: MICCAI, 2013.
[27] B. Dashtbozorg, A. Mendonca, A. Campilho, An automatic graph-based approach for artery/vein classification in retinal images, IEEE Trans. Image Process. 23 (3) (2014) 1073–1083.
[28] G. Azzopardi, N. Petkov, Automatic detection of vascular bifurcations in segmented retinal images using trainable COSFIRE filters, Pattern Recogn. Lett. 34 (8) (2013) 922–933.
[29] T. Kohler, A. Budai, M. Kraus, J. Odstrcilik, G. Michelson, J. Hornegger, Automatic no-reference quality assessment for retinal fundus images using vessel segmentation, in: IEEE Int. Symp. on Computer-Based Medical Systems, 2013, pp. 95–100.
[30] M. Fraz, P. Remagnino, A. Hoppe, B. Uyyanonvara, A. Rudnicka, C. Owen, S. Barman, An ensemble classification-based approach applied to retinal blood vessel segmentation, IEEE Trans. Biomed. Eng. 59 (9) (2012) 2538–2548.
[31] D. Farnell, F. Hatfield, P. Knox, M. Reakes, S. Spencer, D. Parry, S. Harding, Enhancement of blood vessels in digital fundus photographs via the application of multiscale line operators, J. Frankl. Inst. 345 (7) (2008) 748–765.
[32] S. Holm, G. Russell, V. Nourrit, N. McLoughlin, DR HAGIS—a novel fundus image database for the automatic extraction of retinal surface vessels, SPIE J. Med. Imaging 4 (1) (2017) 1–11.

[33] M. Niemeijer, X. Xu, A. Dumitrescu, P. Gupta, B. Ginneken, J. Folk, M. Abramoff, Automated measurement of the arteriolar-to-venular width ratio in digital color fundus photographs, IEEE Trans. Med. Imaging 30 (11) (2011) 1941–1950.
[34] E. Grisan, M. Foracchia, A. Ruggeri, A novel method for the automatic grading of retinal vessel tortuosity, IEEE Trans. Med. Imaging 27 (3) (2008) 310–319.
[35] J. Zhang, B. Dashtbozorg, E. Bekkers, J. Pluim, R. Duits, B. Romeny, Robust retinal vessel segmentation via locally adaptive derivative frames in orientation scores, IEEE Trans. Med. Imaging 35 (12) (2016) 2631–2644.
[36] R. Estrada, M. Allingham, P. Mettu, S. Cousins, C. Tomasi, S. Farsiu, Retinal artery-vein classification via topology estimation, IEEE Trans. Med. Imaging 34 (12) (2015) 2518–2534.
[37] A. Perez-Rovira, R. Cabido, E. Trucco, S. McKenna, J. Hubschman, RERBEE: robust efficient registration via bifurcations and elongated elements applied to retinal fluorescein angiogram sequences, IEEE Trans. Med. Imaging 30 (1) (2012) 140–150.
[38] I. Styles, A. Calcagni, E. Claridge, F. Espina, J. Gibson, Quantitative analysis of multi-spectral fundus images, Med. Image Anal. 10 (4) (2016) 578–597.
[39] O. Russakovsky, J. Deng, H. Su, J. Krause, S. Satheesh, S. Ma, Z. Huang, A. Karpathy, A. Khosla, M. Bernstein, A. Berg, L. Fei-Fei, ImageNet large scale visual recognition challenge, Int. J. Comput. Vis. 115 (3) (2015) 211–252.
[40] T.-Y. Lin, M. Maire, S. Belongie, J. Hays, P. Perona, D. Ramanan, P. Dollar, C.L. Zitnick, Microsoft COCO: common objects in context, in: European Conf. Computer Vision (ECCV), 2014.
[41] X. Jiang, M. Lambers, H. Bunke, Structural performance evaluation of curvilinear structure detection algorithms with application to retinal vessel segmentation, Pattern Recogn. Lett. 33 (2012) 2048–2056.
[42] M. Gegundez-Arias, A. Aquino, J. Bravo, D. Marin, A function for quality evaluation of retinal vessel segmentations, IEEE Trans. Med. Imaging 31 (2) (2012) 231–239.
[43] Z. Yan, X. Yang, K. Cheng, A skeletal similarity metric for quality evaluation of retinal vessel segmentation, IEEE Trans. Med. Imaging 37 (4) (2018) 1045–1057.
[44] E. Trucco, A. Ruggeri, T. Karnowski, L. Giancardo, E. Chaum, J. Hubschman, B. Al-Diri, C. Cheung, D. Wong, M. Abramoff, G. Lim, D. Kumar, P. Burlina, N. Bressler, H. Jelinek, F. Meriaudeau, G. Quellec, T. MacGillivray, B. Dhillon, Validating retinal fundus image analysis algorithms: issues and a proposal, Invest. Ophthalmol. Vis. Sci. 54 (2013) 3546–3559.
[45] A. Galdran, P. Costa, A. Bria, T. Araujo, A. Mendonca, A. Campilho, A no-reference quality metric for retinal vessel tree segmentation, in: MICCAI, 2008.
[46] L. Tramontan, E. Poletti, D. Fiorin, A. Ruggeri, A web-based system for the quantitative and reproducible assessment of clinical indexes from the retinal vasculature, IEEE Trans. Biomed. Eng. 58 (3) (2011) 818–821.
[47] S. Chaudhuri, S. Chatterjee, N. Katz, M. Nelson, M. Goldbaum, Detection of blood vessels in retinal images using two-dimensional matched filters, IEEE Trans. Med. Imaging 8 (3) (1989) 263–269.
[48] A. Pinz, S. Bernogger, P. Datlinger, A. Kruger, Mapping the human retina, IEEE Trans. Med. Imaging 17 (4) (1998) 606–619.
[49] L. Gang, O. Chutatape, S. Krishnan, Detection and measurement of retinal vessels in fundus images using amplitude modified second-order Gaussian filter, IEEE Trans. Med. Imaging 49 (2) (2002) 168–172.

[50] V. Mahadevan, H. Narasimha-Iyer, B. Roysam, H. Tanenbaum, Robust model-based vasculature detection in noisy biomedical images, IEEE Trans. Inf. Technol. Biomed. 8 (3) (2004) 360–376.
[51] M. Sofka, C. Stewart, Retinal vessel centerline extraction using multiscale matched filters, confidence and edge measures, IEEE Trans. Med. Imaging 25 (12) (2006) 1531–1546.
[52] K. Tobin, E. Chaum, P. Govindasamy, T. Karnowski, Detection of anatomic structures in human retinal imagery, IEEE Trans. Med. Imaging 26 (12) (2007) 1729–1739.
[53] A. Mendonca, A. Campilho, Segmentation of retinal blood vessels by combining the detection of centerlines and morphological reconstruction, IEEE Trans. Med. Imaging 25 (9) (2006) 1200–1213.
[54] M. Miri, A. Mahloojifar, Retinal image analysis using curvelet transform and multistructure elements morphology by reconstruction, IEEE Trans. Biomed. Eng. 58 (5) (2011) 1183–1192.
[55] M. Martinez-Perez, A. Hughes, S. Thom, A. Bharath, K. Parker, Segmentation of blood vessels from red-free and fluorescein retinal images, Med. Image Anal. 11 (2007) 47–61.
[56] L. Wang, A. Bhalerao, R. Wilson, Analysis of retinal vasculature using a multiresolution Hermite model, IEEE. Trans. Med. Imaging 26 (2) (2007) 137–152.
[57] P. Bankhead, C. Scholfield, J. McGeown, T. Curtis, Fast retinal vessel detection and measurement using wavelets and edge location refinement, PLoS ONE 7 (3) (2012) e32435.
[58] S. Roychowdhury, D. Koozekanani, K. Parhi, Iterative vessel segmentation of fundus images, IEEE Trans. Biomed. Eng. 62 (7) (2015) 1738–1749.
[59] Y. Xu, T. Geraud, L. Najman, Connected filtering on tree-based shape-spaces, IEEE Trans. Pattern Anal. Mach. Intell. 38 (6) (2016) 1126–1140.
[60] G. Kovacs, A. Hajdu, A self-calibrating approach for the segmentation of retinal vessels by template matching and contour reconstruction, Med. Image Anal. 29 (2016) 24–46.
[61] L. Espona, M. Carreira, M. Penedo, M. Ortega, Retinal vessel tree segmentation using a deformable contour model, in: ICPR, 2008.
[62] B. Al-Diri, A. Hunter, D. Steel, An active contour model for segmenting and measuring retinal vessels, IEEE Trans. Med. Imaging 28 (9) (2009) 1488–1497.
[63] B. Lam, H. Yan, A novel vessel segmentation algorithm for pathological retina images based on the divergence of vector fields, IEEE Trans. Med. Imaging 27 (2) (2008) 237–246.
[64] B. Lam, Y. Gao, A. Liew, General retinal vessel segmentation using regularization-based multiconcavity modeling, IEEE Trans. Med. Imaging 29 (7) (2010) 1369–1381.
[65] K. Sun, Z. Chen, S. Jiang, Local morphology fitting active contour for automatic vascular segmentation, IEEE Trans. Biomed. Eng. 59 (2) (2012) 464–473.
[66] Y. Zhao, X. Wang, X. Wang, F. Shih, Retinal vessels segmentation based on level set and region growing, Pattern Recogn. 47 (7) (2014) 2437–2446.
[67] Y. Zhao, L. Rada, K. Chen, S. Harding, Y. Zheng, Automated vessel segmentation using infinite perimeter active contour model with hybrid region information with application to retinal images, IEEE Trans. Med. Imaging 34 (9) (2015) 1797–1807.
[68] D. Chen, J. Zhang, L. Cohen, Minimal paths for tubular structure segmentation with coherence penalty and adaptive anisotropy, IEEE Trans. Image Process. 28 (2019) 1271–1284.

[69] M. Poon, G. Hamarneh, R. Abugharbieh, Live-vessel: extending livewire for simultaneous extraction of optimal medial and boundary paths in vascular images, in: MICCAI, 2007.
[70] A. Youssry, A. El-Rafei, S. Elramly, A quantum mechanics-based algorithm for vessel segmentation in retinal images, Quantum Inf. Process. 15 (6) (2016) 2303–2323.
[71] C. Sinthanayothin, J. Boyce, H. Cook, T. Williamson, Automated localisation of the optic disc, fovea, and retinal blood vessels from digital colour fundus images, Br. J. Opthalmol. 83 (8) (1999) 902–910.
[72] C. Lupascu, D. Tegolo, E. Trucco, FABC: retinal vessel segmentation using AdaBoost, IEEE Trans. Inf. Technol. Biomed. 14 (5) (2010) 1267–1274.
[73] D. Marin, A. Aquino, M. Gegundez-Arias, J. Bravo, A new supervised method for blood vessel segmentation in retinal images by using gray-level and moment invariants-based features, IEEE Trans. Med. Imaging 30 (1) (2011) 146–158.
[74] E. Ricci, R. Perfetti, Retinal blood vessel segmentation using line operators and support vector classification, IEEE. Trans. Med. Imaging 26 (10) (2007) 1357–1365.
[75] C. Becker, R. Rigamonti, V. Lepetit, P. Fua, Supervised feature learning for curvilinear structure segmentation, in: Medical Image Computing and Computer-Assisted Interventation (MICCAI), 2013.
[76] G. Azzopardi, N. Strisciuglio, M. Vento, N. Petkov, Trainable COSFIRE filters for vessel delineation with application to retinal images, Med. Image Anal. 19 (1) (2015) 46–57.
[77] G. Azzopardi, N. Petkov, Trainable COSFIRE filters for keypoint detection and pattern recognition, IEEE Trans. Pattern Anal. Mach. Intell. 35 (2) (2013) 490–503.
[78] J. Soares, J. Leandro, R. Cesar, H. Jelinek, M. Cree, Retinal vessel segmentation using the 2-D Gabor wavelet and supervised classification, IEEE Trans. Med. Imaging 25 (9) (2006) 1214–1222.
[79] R. Rigamonti, V. Lepetit, Accurate and efficient linear structure segmentation by leveraging ad hoc features, in: MICCAI, 2012.
[80] E. Turetken, F. Benmansour, B. Andres, H. Pfister, P. Fua, Reconstructing loopy curvilinear structures using integer programming, in: CVPR, 2014.
[81] C. Becker, R. Rigamonti, V. Lepetit, P. Fua, Supervised feature learning for curvilinear structure segmentation, in: MICCAI, 2013.
[82] J. Orlando, M. Blaschko, Learning fully-connected CRFs for blood vessel segmentation in retinal images, in: MICCAI, 2014.
[83] J. Orlando, E. Prokofyeva, M. Blaschko, A discriminatively trained fully connected conditional random field model for blood vessel segmentation in fundus images, IEEE Trans. Biomed. Eng. 64 (1) (2017) 16–27.
[84] X. You, Q. Peng, Y. Yuan, Y. Cheung, J. Lei, Segmentation of retinal blood vessels using the radial projection and semi-supervised approach, Pattern Recogn. 44 (10–11) (2011) 2314–2324.
[85] L. Gu, L. Cheng, Learning to boost filamentary structure segmentation, in: ICCV, 2015.
[86] Y. Ganin, V. Lempitsky, N4-Fields: neural network nearest neighbor fields for image transforms, in: Asian Conference on Computer Vision, 2014, pp. 536–551.
[87] P. Liskowski, K. Krawiec, Segmenting retinal blood vessels with deep neural networks, IEEE Trans. Med. Imaging 35 (11) (2016) 2369–2380.
[88] Q. Li, B. Feng, L. Xie, P. Liang, H. Zhang, T. Wang, A cross-modality learning approach for vessel segmentation in retinal images, IEEE Trans. Med. Imaging 35 (1) (2016) 109–118.

[89] H. Fu, Y. Xu, S. Lin, D. Wong, J. Liu, DeepVessel: retinal vessel segmentation via deep learning and conditional random field, in: MICCAI, 2016.
[90] Z. Yan, X. Yang, K. Cheng, Joint segment-level and pixel-wise losses for deep learning based retinal vessel segmentation, IEEE Trans. Biomed. Eng. 65 (9) (2018) 1912–1923.
[91] K. Maninis, J. Pont-Tuset, P. Arbelaez, L. Gool, Deep retinal image understanding, in: MICCAI, 2016.
[92] H. Zhao, H. Li, S. Maurer-Stroh, L. Cheng, Synthesizing retinal and neuronal images with generative adversarial nets, Med. Image Anal. 49 (2018) 14–26.
[93] H. Zhao, H. Li, S. Maurer-Stroh, Y. Guo, Q. Deng, L. Cheng, Supervised segmentation of un-annotated retinal fundus images by synthesis, IEEE Trans. Med. Imaging 38 (1) (2018) 46–56.
[94] R. Frangi, W. Niessen, K. Vincken, M. Viergever, Multiscale vessel enhancement filtering, in: Medical Image Computing and Computer-Assisted Interventation (MICCAI), 1998, pp. 130–137.
[95] F. Zana, J. Klein, Segmentation of vessel-like patterns using mathematical morphology and curvature evaluation, IEEE Trans. Image Proc. 10 (7) (2001) 1010–1019.
[96] F. Benmansour, L. Cohen, Tubular structure segmentation based on minimal path method and anisotropic enhancement, Int. J. Comput. Vis. 92 (2) (2011) 192–210.
[97] A. Sironi, V. Lepetit, P. Fua, Segmentation of the surfaces of the retinal layer from OCT images, in: ICCV, 2015.
[98] A. Sironi, E. Turetken, V. Lepetit, P. Fua, Multiscale centerline detection, IEEE Trans. Pattern Anal. Mach. Intell. 38 (7) (2016) 1327–1341.
[99] R. Annunziata, E. Trucco, Accelerating convolutional sparse coding for curvilinear structures segmentation by refining SCIRD-TS filter banks, IEEE Trans. Med. Imaging 35 (11) (2016) 2381–2392.
[100] L. Gu, X. Zhang, H. Zhao, H. Li, L. Cheng, Segment 2D and 3D filaments by learning structured and contextual features, IEEE Trans. Med. Imaging 36 (2) (2017) 569–606.
[101] L. Cohen, T. Deschamps, Grouping connected components using minimal path techniques. Application to reconstruction of vessels in 2D and 3D images, in: IEEE Conference on Computer Vision and Pattern Recognition (CVPR), 2001.
[102] M. Pechaud, R. Keriven, G. Peyre, Extraction of tubular structures over an orientation domain, in: IEEE Conference on Computer Vision and Pattern Recognition (CVPR), 2009.
[103] W. Liao, S. Worz, C. Kang, Z. Cho, K. Rohr, Progressive minimal path method for segmentation of 2D and 3D line structures, IEEE Trans. Pattern Anal. Mach. Intell. 40 (3) (2018) 696–709.
[104] S. Yamamoto, H. Yokouchi, Automatic recognition of color fundus photographs, in: K. Preston, M. Onoe (Eds.), Digital Processing of Biomedical Images, Springer, Berlin, 1976.
[105] D. Calvo, M. Ortega, M. Penedo, J. Rouco, Vascular intersection detection in retina fundus images using a new hybrid approach, Comput. Biol. Med. 40 (1) (2010) 81–89.
[106] S. Yamamoto, H. Yokouchi, Automatic recognition of color fundus photographs, Dig. Process. Biomed. Images 103 (1) (2011) 28–38.
[107] B. Al-Diri, A. Hunter, D. Steel, M. Habib, Automated analysis of retinal vascular network connectivity, Comput. Med. Imaging Graph. 34 (6) (2010) 462–470.
[108] T. Qureshi, A. Hunter, B. Al-Diri, A Bayesian framework for the local configuration of retinal junctions, in: CVPR, 2014.

[109] S. Tamura, Y. Okamoto, K. Yanashima, Zero-crossing interval correction in tracing eye-fundus blood vessels, Pattern Recogn. 21 (3) (1988) 227–233.
[110] A. Can, H. Shen, J. Taylor, H. Tanenbaum, B. Roysam, Rapid automated tracing and feature extraction from retinal fundus images using direct exploratory algorithm, IEEE Trans. Inf. Tech. Biomed. 3 (2) (1999) 125–138.
[111] C. Tsai, C. Stewart, H. Tanenbaum, B. Roysam, Model-based method for improving the accuracy and repeatability of estimating vascular bifurcations and crossovers from retinal fundus images, IEEE Trans. Inf. Technol. Biomed. 8 (2) (2004) 122–130.
[112] T. Yedidya, R. Hartley, Tracking of blood vessels in retinal images using Kalman filter, in: DICTA, 2008.
[113] K.S. Lin, C.L. Tsai, C.H. Tsai, M. Sofka, S.J. Chen, W.Y. Lin, Retinal vascular tree reconstruction with anatomical realism, IEEE Trans. Biomed. Eng. 59 (12) (2012) 3337–3347.
[114] J. De, T. Ma, H. Li, M. Dash, L. Cheng, Automated tracing of retinal blood vessels using graphical models, in: Scandinavian Conference on Image Analysis, 2013.
[115] J. De, H. Li, L. Cheng, Tracing retinal vessel trees by transductive inference, BMC Bioinformatics 15 (20) (2014) 1–20.
[116] L. Cheng, J. De, X. Zhang, F. Lin, H. Li, Tracing retinal blood vessels by matrix-forest theorem of directed graphs, in: MICCAI, 2014.
[117] J. De, L. Cheng, X. Zhang, F. Lin, H. Li, K. Ong, W. Yu, Y. Yu, S. Ahmed, A graph-theoretical approach for tracing filamentary structures in neuronal and retinal images, IEEE Trans. Med. Imaging 35 (1) (2016) 257–272.
[118] J. De, X. Zhang, F. Lin, L. Cheng, Transduction on directed graphs via absorbing random walks, IEEE Trans. Pattern Anal. Mach. Intell. 40 (7) (2018) 1770–1784.
[119] Q. Lau, M. Lee, W. Hsu, T. Wong, Simultaneously identifying all true vessels from segmented retinal images, IEEE Trans. Biomed. Eng. 60 (7) (2013) 1851–1858.
[120] X. Lyu, Q. Yang, S. Xia, S. Zhang, Construction of retinal vascular trees via curvature orientation prior, in: IEEE International Conference on Bioinformatics and Biomedicine, 2016.
[121] E. Bekkers, R. Duits, T. Berendschot, B.M. ter Haar Romeny, A multi-orientation analysis approach to retinal vessel tracking, J. Math. Imaging Vis. 49 (3) (2014) 583–610.
[122] E. Bekkers, R. Duits, A. Mashtakov, Y. Sachkov, Vessel tracking via sub-Riemannian geodesics on the projective line bundle, in: International Conference on Geometric Science of Information, 2017.
[123] E. Bekkers, D. Chen, J. Portegies, Nilpotent approximations of sub-Riemannian distances for fast perceptual grouping of blood vessels in 2D and 3D, J. Math. Imaging Vis. 60 (2018) 882–899.
[124] S. Abbasi-Sureshjani, M. Favali, G. Citti, A. Sarti, B.M. ter Haar Romeny, Curvature integration in a 5D kernel for extracting vessel connections in retinal images, IEEE Trans. Image Process. 27 (2) (2018) 606–621.
[125] J. Zhang, E. Bekkers, D. Chen, T. Berendschot, J. Schouten, J. Pluim, Y. Shi, B. Dashtbozorg, B.M. ter Haar Romeny, Reconnection of interrupted curvilinear structures via cortically inspired completion for ophthalmologic images, IEEE Trans. Biomed. Eng. 65 (5) (2018) 1151–1165.
[126] C. Ventura, J. Pont-Tuset, S. Caelles, K. Maninis, L.V. Gool, Iterative deep retinal topology extraction, in: International Workshop on Patch-Based Techniques in Medical Imaging, 2018.

[127] F. Uslu, A. Bharath, A multi-task network to detect junctions in retinal vasculature, in: MICCAI, 2018.
[128] F. Caliva, A. Hunter, P. Chudzik, G. Ometto, L. Antiga, B. Al-Diri, A fluid-dynamic based approach to reconnect the retinal vessels in fundus photography, in: International Conference of the IEEE Engineering in Medicine and Biology Society, 2017.
[129] H. Shen, B. Roysam, C. Stewart, J. Turner, H. Tanenbaum, Optimal scheduling of tracing computations for real-time vascular landmark extraction from retinal fundus images, IEEE Trans. Inf. Technol. Biomed. 5 (1) (2001) 77–91.
[130] K. Al-Kofahi, S. Lasek, D. Szarowski, C. Pace, G. Nagy, J. Turner, B. Roysam, Rapid automated three-dimensional tracing of neurons from confocal image stacks, IEEE Trans. Inf. Tech. Biomed. 6 (2) (2002) 171–187.
[131] K. Brown, G. Barrionuevo, A. Canty, V.D. Paola, J. Hirsch, G. Jefferis, J. Lu, M. Snippe, I. Sugihara, G. Ascoli, The DIADEM data sets: representative light microscopy images of neuronal morphology to advance automation of digital reconstructions, Neuroinformatics 9 (2011) 143–157.
[132] M. Radojevic, E. Meijering, Automated neuron tracing using probability hypothesis density filtering, Bioinformatics 33 (7) (2017) 1073–1080.
[133] M. Martinez-Perez, A. Hughes, A. Stanton, S. Thom, N. Chapman, A. Bharath, K. Parker, Retinal vascular tree morphology: a semi-automatic quantification, IEEE Trans. Biomed. Eng. 49 (8) (2002) 912–917.
[134] K. Rothaus, X. Jiang, P. Rhiem, Separation of the retinal vascular graph in arteries and veins based upon structural knowledge, Image Vis. Comput. 27 (7) (2009) 864–875.
[135] H. Narasimha-Iyer, J. Beach, B. Khoobehi, B. Roysam, Automatic identification of retinal arteries and veins from dual-wavelength images using structural and functional features, IEEE Trans. Biomed Eng. 54 (8) (2007) 1427–1435.
[136] E. Turetken, C. Blum, G. Gonzalez, P. Fua, Reconstructing geometrically consistent tree structures from noisy images, in: Medical Image Computing and Computer-Assisted Interventation (MICCAI), 2010.
[137] E. Pellegrini, G. Robertson, T. MacGillivray, J. van Hemert, G. Houston, E. Trucco, A graph cut approach to artery/vein classification in ultra-widefield scanning laser ophthalmoscopy, IEEE Trans. Med. Imaging 37 (2) (2018) 516–526.
[138] V. Joshi, J. Reinhardt, M. Garvin, M. Abramoff, Automated method for identification and artery-venous classification of vessel trees in retinal vessel networks, PLoS ONE 9 (2) (2014) 1–12.
[139] M. Niemeijer, X. Xu, A. Dumitrescu, P. Gupta, B.V. Ginneken, J. Folk, M. Abramoff, Automated measurement of the arteriolar-to-venular width ratio in digital color fundus photographs, IEEE Trans. Med. Imaging 30 (11) (2011) 1941–1950.
[140] U. Nguyen, A. Bhuiyan, L. Park, R. Kawasaki, T. Wong, J. Wang, P. Mitchell, K. Ramamohanarao, An automated method for retinal arteriovenous nicking quantification from color fundus images, IEEE Trans. Biomed. Eng. 60 (11) (2013) 3194–3203.
[141] M. Aghamohamadian-Sharbaf, H. Pourreza, T. Banaee, A novel curvature-based algorithm for automatic grading of retinal blood vessel tortuosity, IEEE J. Biomed. Health Inform. 20 (2) (2016) 586–595.
[142] M. Adam, W. Aenchbacher, T. Kurzweg, J. Hsu, Plenoptic ophthalmoscopy: a novel imaging technique, Ophthalmic Surg. Lasers Imaging Retina 9 (7) (2018) 3178–3192.
[143] M. Haeker, M. Abramoff, R. Kardon, M. Sonka, Segmentation of the surfaces of the retinal layer from OCT images, in: MICCAI, 2006.

[144] M. Garvin, M. Abramoff, R. Kardon, S. Russell, X. Wu, M. Sonka, Intraretinal layer segmentation of macular optical coherence tomography images using optimal 3-D graph search, IEEE Trans. Med. Imaging 27 (10) (2008) 1495–1505.
[145] M. Niemeijer, M. Garvin, B. van Ginneken, M. Sonka, M. Abramoff, Vessel segmentation in 3D spectral OCT scans of the retina, in: SPIE Medical Imaging: Image Processing, 2008.
[146] A. Fuller, R. Zawadzki, S. Choi, D. Wiley, J. Werner, B. Hamann, Segmentation of three-dimensional retinal image data, IEEE Trans. Vis. Comput. Graph. 13 (6) (2007) 1719–1726.
[147] P. Guimaraes, P. Rodrigues, D. Celorico, P. Serranho, R. Bernardes, Three-dimensional segmentation and reconstruction of the retinal vasculature from spectral-domain optical coherence tomography, J. Biomed. Opt. 20 (1) (2015) 1–11.
[148] Z. Hu, M. Niemeijer, M. Abramoff, M. Garvin, Multimodal retinal vessel segmentation from spectral-domain optical coherence tomography and fundus photography, IEEE Trans. Med. Imaging 31 (10) (2012) 1900–1911.
[149] R. Kafieh, H. Rabbani, F. Hajizadeh, M. Ommani, An accurate multimodal 3-D vessel segmentation method based on brightness variations on OCT layers and curvelet domain fundus image analysis, IEEE Trans. Biomed. Eng. 60 (10) (2013) 2815–2823.
[150] N. Panwar, P. Huang, J. Lee, P. Keane, T. Chuan, A. Richhariya, S. Teoh, T. Lim, R. Agrawal, Fundus photography in the 21st century—a review of recent technological advances and their implications for worldwide healthcare, Telemed. e-Health 22 (3) (2016) 198–208.
[151] D. Palmer, T. Coppin, K. Rana, D. Dansereau, M. Suheimat, M. Maynard, D. Atchison, J. Roberts, R. Crawford, A. Jaiprakash, Glare-free retinal imaging using a portable light field fundus camera, Biomed. Opt. Express 47 (11) (2016) 1038–1043.
[152] M. Hajabdollahi, R. Esfandiarpoor, S. Soroushmehr, N. Karimi, S. Samavi, K. Najarian, Low complexity convolutional neural network for vessel segmentation in portable retinal diagnostic devices, in: International Conference on Image Processing, 2018.